A simplified monitoring model for PMSM servoactuator prognostics

A simplified monitoring model for PMSM servoactuator prognostics

Pier Carlo Berri[1], *Matteo D.L.* Dalla Vedova[1,*], *Paolo* Maggiore[1], and *Francesco* Viglione[1]

[1]Dept. of Mechanical & Aerospace Engineering (DIMEAS), Politecnico di Torino, Turin, Italy

Abstract. Electromechanical actuators (EMAs) based on Permanent Magnet Synchronous Motors (PMSMs) are currently employed on various aircraft systems, and are becoming more and more widespread in safety critical applications. Compared to other electrical machines, PMSM offer a high power to weight ratio and low cogging: this makes them suited for position control and actuation tasks. EMAs offer several advantages over hydraulic servoactuators, in terms of modularity, mechanical simplicity, overall weight and fuel efficiency. At the same time, their basic reliability is inherently lower compared to hydraulic actuators. Then, the use of EMAs for safety critical aircraft systems requires the adoption of risk mitigation techniques to counter this issue. In this framework, diagnostic and prognostic strategies can be used for the system health management, to monitor its behaviour in search of the early signs of the most common or dangerous failure modes. We propose a low fidelity model of a PMSM based EMA, intended for model-based diagnostic and prognostic monitoring. The model features low computational cost, allowing the execution in nearly real-time, combined with suitable accuracy in the simulation of faulty system operations. This simplified emulator is validated by comparing its behaviour to a higher fidelity model, employed as a simulated test bench.

1 Introduction

Multifidelity approaches to prognostics involve using and developing models of the monitored system with varying levels of accuracy and computational complexity, and different application domains [1-4]. As an example, complex high fidelity models are used to train the machine learning tools employed for fault detection. These models can be similar in complexity to those used in the system design phase, but while the latter focus on the nominal system operations, prognostics models are intended to accurately simulate the effect of faults on system performance. Lower fidelity models are typically employed in model-based Fault Detection and Identification (FDI) [5-8], where a moderate-to-high accuracy is required combined with a low computational complexity. For example, fault detection based on meta-heuristic optimization [9-12] requires a model of the system faults able to be executed iteratively in a reasonable time, in order to match the model response to the actual system and provide an estimate of its health condition.

* Corresponding author: matteo.dallavedova@polito.it

In this work we focus on the FDI task for a Permanent Magnet Synchronous Motor (PMSM) Electromechanical Actuator (EMA), and we propose a simplified model of the servo system, intended for prognostic tasks. Electromechanical actuators are being considered for aircraft flight control systems [13, 14], but issues regarding their reliability still limit their diffusion on safety critical applications [15]. For this reason, prognostics is often regarded as an enabling factor for the widespread diffusion of EMAs in aeronautics.

1.1 EMA architecture and Fault Modes

Referring to Figure 1, a typical EMA architecture involves an Actuator Control Electronics (ACE) module, which compares the position command to the actual position measured by sensors, to compute a current command for the power electronics module. The Power Electronics convert the DC or AC electrical power supply into the required three-phase power for the PMSM, with the required frequency and amplitude depending on the command and rotor angular position. A mechanical transmission connects the motor to the controlled component on which external load is applied. The transmission usually consists in a reduction gearbox (planetary or ordinary) and a device for converting rotary motion into linear motion. For this purpose, ball-screws and roller-screws are preferred over lead screws for their higher efficiency, and over rack-and-pinion for their lower backlash and higher specific load. Eventually, a network of sensors is used to close the feedback loops. A resolver on the motor shaft is needed for actuating the commutation sequence, while Rotary Variable Differential Transducers (RVDTs) or Linear Variable Differential Transducers (LVDTs) on the transmission output provide absolute position information for the control loop. Current sensors are used for closing the inner current loop and provide torque control, while the motor speed can be measured by a dedicated sensor or computed as the derivative of motor position.

We consider five different failure modes among the most likely to occur on electromechanical systems, according to a work by Edward Balaban et al. [16]. In particular, an increase of friction may be caused by wear of the gearbox or degradation of the lubricant; an increase of backlash is due mainly to ballscrew thread degradation. As regards the motor, partial short circuit and rotor eccentricity may be caused by the degradation of the winding insulation and rotor bearings respectively. Eventually, a controller gain drift may be the result of degradation of analog electronics, overheating of components, drift of the reference voltage for analog-to-digital conversion, or drift of position transducer gains.

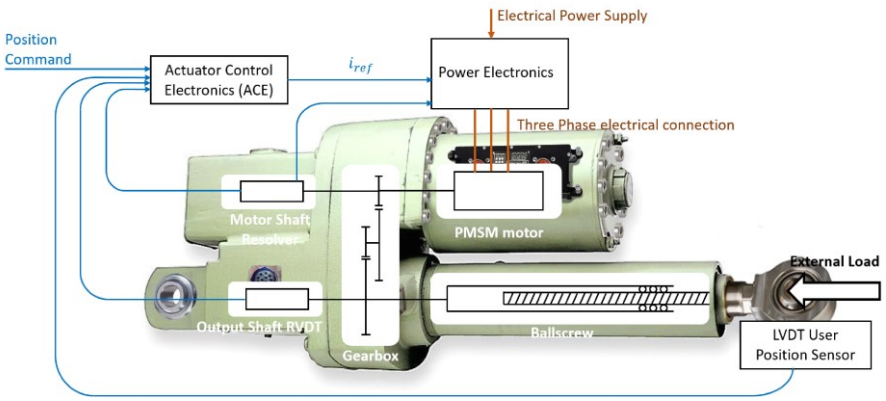

Fig. 1. Typical architecture of an Electromechanical actuator for flight controls.

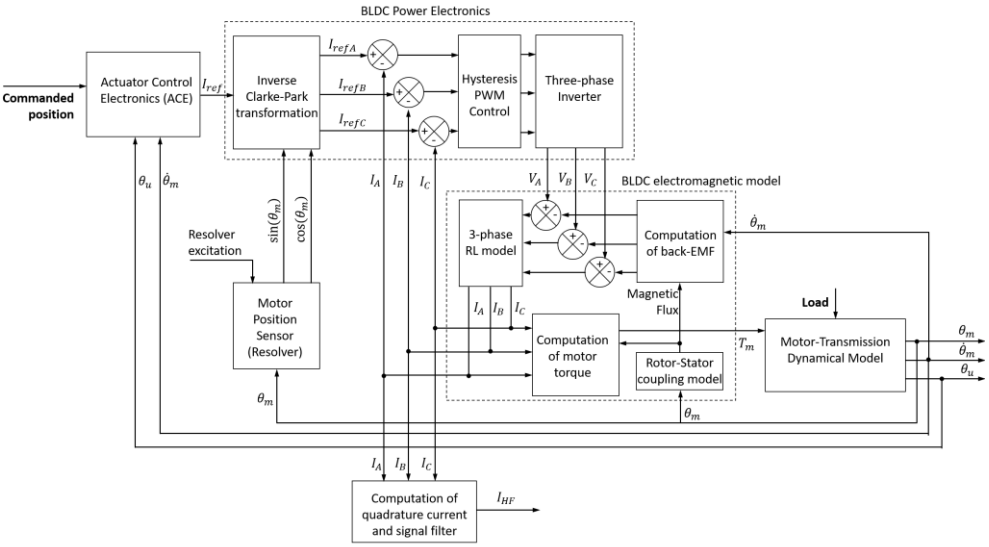

Fig. 2. Block diagram of the High Fidelity EMA model. Despite being a lumped parameters model, the simulation is very accurate but computationally intensive (two orders of magnitude above real-time).

2 High Fidelity (HF) model

We start from a complex and detailed High Fidelity (HF) model, initially presented in [17, 18], and schematically represented in the block diagram of Figure 2.

This model, implemented in the Matlab-Simulink simulation environment, accounts for several aspects of the EMA operations from a physical point of view. The three-phase RL stator circuit, the hysteresis current control, as well as the magnetic coupling between rotor and stator are modelled analytically, starting from the well-known physical governing equations of dynamics and electromagnetism, and employing a lumped parameter representation of the components. Electromagnetic and mechanical FEM are not employed, since their use would require a computational time not compatible with a dynamical model, even a high fidelity one. This approach allows for an accurate simulation of the actual EMA, and has been validated with data available in literature; however, the resulting model is quite computationally intensive and not suitable for iterative evaluation within FDI algorithms. The motor-transmission dynamical model is a second order model accounting for several nonlinearities, such as dry friction (modelled as proposed by [19] and assessed in [20]), backlash, and mechanical end-stops.

The most computationally expensive section is the three-phase RL model: the short RL characteristic time requires a very short integration time step (below one microsecond for the particular EMA taken into account) to guarantee numerical stability. At the same time, the three-phase star-connected circuit may be unbalanced as an effect of electrical faults. Then, the standard delta-star conversion cannot be applied and the voltage of the floating neutral node is computed iteratively at each time step; the task is performed by the Sim Power System Simulink solver, and accounts for most of the required computational time.

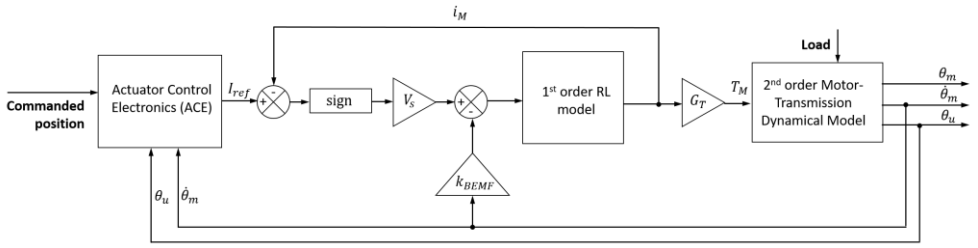

Fig. 3. Block diagram of the Low Fidelity EMA model

As a result, the computational time of the HF model is almost two orders of magnitude above real-time, meaning that one second of simulation time translates into about one minute of computing time on an average laptop PC. This is totally incompatible with iterative execution for FDI in a real operating scenario, since a single fault identification would require several hours.

3 Low Fidelity (LF) model: assumptions and architecture

In this work, we present a simplified model of the considered EMA, intended for online nearly real-time monitoring and fault detection tasks. The main assumption taken into account is to treat the PMSM as an equivalent single-phase motor, with a simple first order dynamical model and equivalent electrical and mechanical characteristics. The most important signal to monitor for EMA FDI is the motor current [17-22], as it is sensitive to a number of fault modes. As a result of the model simplifying assumptions, three-phase current signals are not available in the monitoring model; we choose to calibrate the model in order to compare the single-phase equivalent current of the monitor with the quadrature current of the PMSM, since both quantities are proportional to the motor torque. The actual quadrature current I_q, as opposed to the commanded one, is computed through the Clarke-Park transformation applied to the measured current signals I_A, I_B, I_C:

$$\begin{Bmatrix} I_d \\ I_q \end{Bmatrix} = \begin{bmatrix} \cos\theta_e & -\sin\theta_e \\ \sin\theta_e & \cos\theta_e \end{bmatrix} \begin{bmatrix} 1 & -1/2 & -1/2 \\ 0 & \sqrt{3}/2 & -\sqrt{3}/2 \end{bmatrix} \begin{Bmatrix} I_A \\ I_B \\ I_C \end{Bmatrix} = [P][C] \begin{Bmatrix} I_A \\ I_B \\ I_C \end{Bmatrix} \quad (1)$$

where [P] and [C] are the Park matrix and the Clarke matrix respectively, and I_d is the direct current. The block diagram of Figure 3 reports the architecture of the simplified model. All the complex PMSM and power electronics models are replaced with a first order model with a simplified hysteresis current loop.

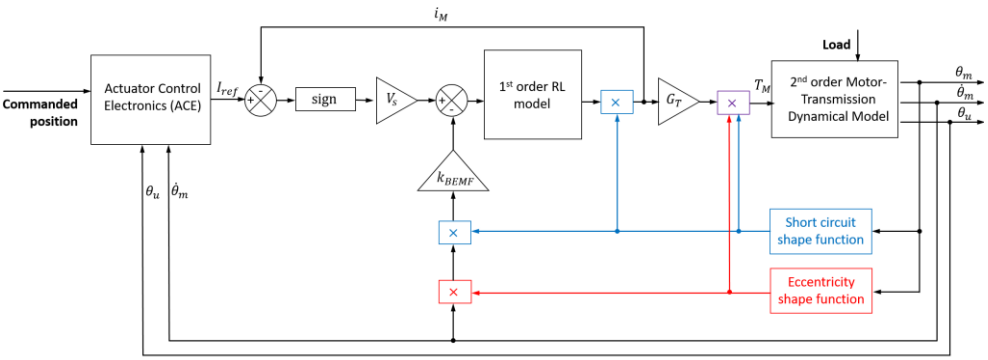

Fig. 4. Placement of the shape functions for electrical faults simulation in the LF model

As regards the simulation of faults, mechanical and control faults can be simulated directly as in the HF model, since the subsystems they act on are mostly unchanged. On the other hand, electrical faults require a surrogate modeling approach. We use shape functions [21, 22] to modulate the motor back-EMF coefficient, resistance, and torque gain as a function of the rotor angular position.

The shape functions are not representative of a particular physical behavior, but are built with the purpose of emulating the behavior of the detailed model, with a lower computational cost. The simplified model is then modified as shown in Figure 4. Both the eccentricity and short circuit shape functions are combinations of sine waves, which depend on the fault magnitude, the rotor angular position, and some calibration coefficients. We define the short circuit shape function as:

$$\varphi_{SC} = k_{FT} \{N_A [1+k_{FS} \sin^2(\theta_e+\pi)] + N_B [1+k_{FS} \sin^2(\theta_e+\pi/3)] + N_C [1+k_{FS} \sin^2(\theta_e-\pi/3)]\} \quad (2)$$

where N_A, N_B, N_C are the fractions of undamaged windings of each phase, k_{FT} and k_{FS} are the global and single contribution calibration coefficients, and θ_e is the rotor electrical angular position. The eccentricity shape function is:

$$\varphi_{ECC} = 1 - k_E \zeta [\cos(\theta_e + \phi_e)] \quad (3)$$

where ζ and ϕ_e are the eccentricity amplitude and direction respectively, and k_E is the eccentricity calibration coefficient.

4 Calibration of the LF model

The short circuit global and single contribution calibration coefficients, the eccentricity calibration coefficient, as well as the equivalent torque gain and back-EMF coefficient of the monitoring model are initially unknown. Their values are obtained through a calibration based on a Genetic Algorithm (GA), which objective function is the Normalized Root Mean Square Error (NRMSE) between the current signals of the two models.

The calibration is a two-steps procedure. In the first step, the models are executed in nominal conditions to determine the optimal values of the equivalent torque gain and back-EMF coefficient. Then, the PMSM electrical characteristics are frozen and the electrical faults are injected into the models; in this phase the GA finds the optimal values for the calibration coefficients of the shape functions. This process is repeated several times with different fault combinations and magnitudes, and the resulting coefficients are averaged.

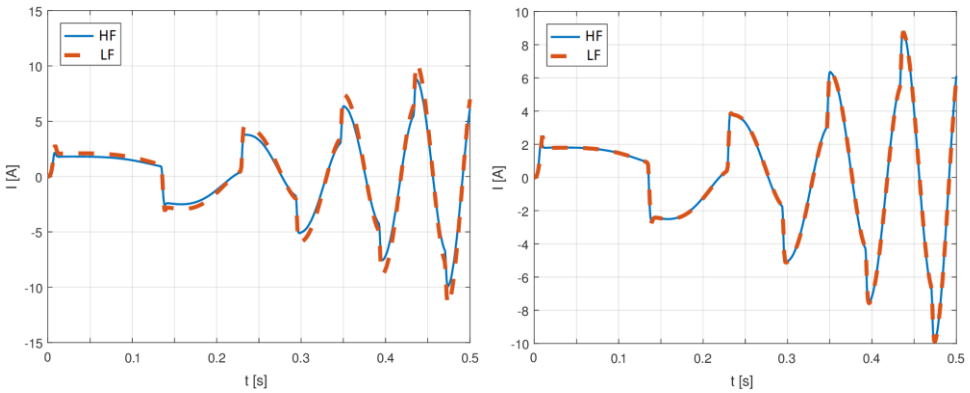

Fig. 5. Comparison of the HF and LF equivalent current signals for a standard chirp position command, in nominal conditions, before (left) and after the first calibration step (right).

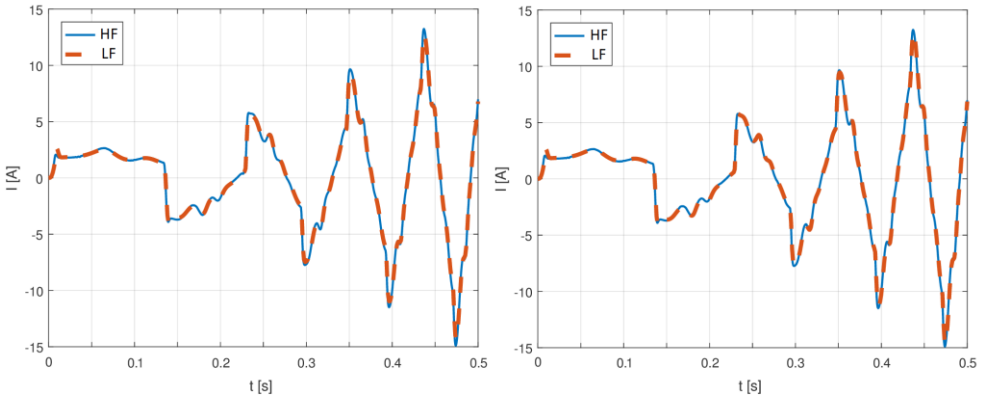

Fig. 6. Comparison of the HF and LF equivalent current signals for a standard chirp position command, with 50% short circuit of phase A, before (left) and after the second calibration step (right).

Splitting the calibration into two phases allows to reduce the dimensionality of the problem for the GA search, greatly reducing the required computational time. This is possible since the fault shape functions have no effect on the simulations when the system is set to nominal conditions.

After the calibration, the current curve matches the reference one with high accuracy, as we can see in Figure 5 (first step of calibration) and Figure 6 (second step of calibration). The first calibration in nominal conditions allows reducing the NRMSE to about 20% of that obtained with the first guess parameters. After the second step, the error is further reduced by another 30%; however, being the discrepancy between the two curves already small, the improvement between left and right graphs of Figure 6 is small.

5 Model validation

To assess the performance of the simplified model and determine its accuracy in reproducing the output of the HF model, we collect a validation dataset containing the result of 100 simulations of the detailed model. Each simulation corresponds to a different fault combination, with a standard chirp position command and a no-load operating condition.

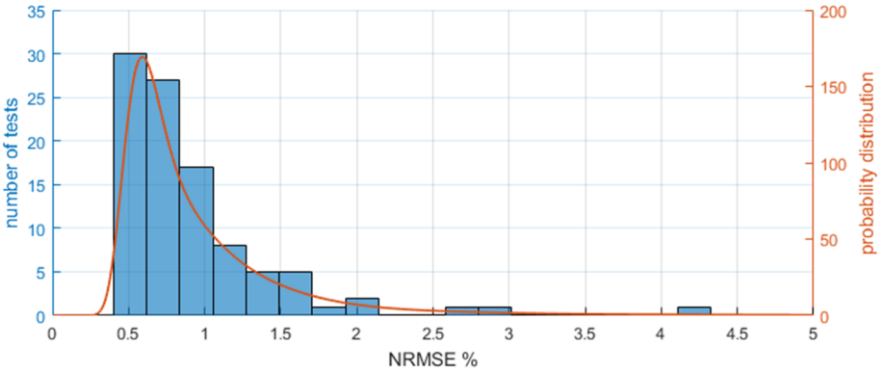

Fig. 6. Statistical distribution of the NRMSE between the HF and LF current signals.

The fault combinations are randomly sampled in the 8-dimensional space of the fault parameters, with a non-uniform distribution. As long as the model is intended for prognostic FDI, maximum accuracy is needed near the nominal condition, i.e. for small, incipient faults. For this reason, we rescale the initial uniform sampling as proposed in [3].

Figure 7 is the distribution of the NRMSE for the 100 validation tests. We can see an average error smaller than 1%, which denotes a high accuracy. Previous works [3, 23] observed a successful FDI with discrepancies as high as 4 to 5%, then the accuracy of the proposed monitoring model is considered adequate. The computational cost has been reduced by almost two orders of magnitude, taking a few seconds of computational time for each second of simulation time. The model is still not executable in real time, but the slow propagation rate of the faults allows to perform the FDI task with a relatively low frequency, e.g. once every some tenths of seconds.

6 Conclusions

A simplified dynamical model of a PMSM-based EMA has been developed and tested, reducing the computational time of more than one order of magnitude. At the same time, we were able to retain a high accuracy of the simulation, comparable to that of the HF model and adequate for diagnostic and prognostic monitoring of the system.

The model will be employed in a future work for FDI tasks with model based meta-heuristic approaches, and will be validated on data coming from a physical experimental test bench, currently under development.

References

1. G. Vachtsevanos, F.L. Lewis, M. Roemer, A. Hess, B. Wu, *Intelligent Fault Diagnosis and Prognosis for Engineering Systems* (John Wiley & Sons, 2008)
2. B. Tasic, J.J. Dohmen, R. Janssen, J.T. Maten, T.G. Beelen, R. Pulch,. *2016 Design, Automation & Test in Europe Conf. & Exhibit. (DATE)*, 301-306 (2016)
3. P.C. Berri, M.D.L. Dalla Vedova, L. Mainini, *AIAA Scitech Forum (AIAA Paper 2019-2210)* (2019)
4. K. Li, Y. Wu, S. Song, Y. Sun, J. Wang, Y. Li, *Proc. Inst. Mechanical Engineers, Part G: J. of Aerospace Engineering*, **231**(1) 98–108 (2017)
5. B. Sohlberg, Y. Aloto, A. Erdogan, E. Erdogan, IFAC Proceedings Volumes **43**(9) 7-12 (2010)
6. Y. Seung-Han, C. Young Man, H. Jin-Oh, Int. J. of Automotive Tech. **18**(3) 405-416 (2017)
7. B. Lee, N. Jeon, H. Lee, *IECON 2012 - 38th Annual Conf. on IEEE Industrial Electronics Soc*. 5376-5381 (2012)
8. A. Hwas, R. Katebi, *Proc. 2012 UKACC Int. Conf. on Control* 876-881 (2012)
9. Y. Kobayashi, L. Song, M. Tomita, P. Chen, MDPI Sensors **19** 3553 (2019)
10. A. Baid, A. K. Srivastava, Students Conf. on Eng. & Systems (SCES) 1-4 (2013)
11. S. Sahu and D. R. Parhi, Applied Mechanics and Materials, **592-594** 2016-2020 (2014)
12. V. Gomathy, S. Selvaperumal, J. of Power Electronics **16**(3) (2016)
13. A. Garcia Garriga, P. Govindaraju, S.S. Ponnusamy, N. Cimmino, L. Mainini, Transportation Research Procedia **29** 146-156 (2018)
14. A. De Martin, G. Jacazio, G. Vachtsevanos, Int. J. of Prognostics and Health Management (2017)

15. G. Pozzuto, A. De Martin, G. Pispola, M. Palmieri, F. Gallorin, *More Electric Aircraft* (Tolouse, 2019)
16. E. Balaban, A. Saxena, K. Goebel, C.S. Byington, S.P. Bharadwaj, M. Smith, *Proc. Annual Conference of the PHM Society* (2009)
17. P.C. Berri, M.D.L. Dalla Vedova, P. Maggiore, M. Scanavino, *2nd European Conference on Electrical Engineering & Computer Science EECS* (2018)
18. M.D.L. Dalla Vedova, P. Maggiore, M. Scanavino, WSEAS Transactions on Power Systems **12** 102-106 (2017)
19. L. Borello, M.D.L. Dalla Vedova (2006). Int. J. of Mechanics and Control (JoMaC) **7**(1), 19-30 (2006)
20. M.D.L. Dalla Vedova, L. Borello, G. Villero, P. Maggiore, *27th Congress of the International Council of the Aeronautical Science* (2010)
21. P.C. Berri, M.D.L. Dalla Vedova, P. Maggiore, Int. J. of Mechanics and Control (JoMaC) **17**(2) 19-25 (2016)
22. P.C. Berri, M.D.L. Dalla Vedova, P. Maggiore, *MATEC Web of Conferences* **233**:00016 (2018)
23. P.C. Berri, M.D.L. Dalla Vedova, L. Mainini, *Proc. 6th European Conf. on Computational Mechanics (ECCM)* (2018)